

Leaf wax and Sr-Nd isotope evidence for high-latitude dust input to the central South China sea and its implication for fertilization

Yang, Yi; Bendle, James A.; Pancost, Richard D.; Yan, Yan; Ruan, Xiaoyan; Warren, Bridget; Lü, Xiaoxia; Li, Xuejie; Yao, Yongjian; Huang, Xianyu; Yang, Huan; Xie, Shucheng

DOI:

[10.1029/2020gl091853](https://doi.org/10.1029/2020gl091853)

License:

None: All rights reserved

Document Version

Peer reviewed version

Citation for published version (Harvard):

Yang, Y, Bendle, JA, Pancost, RD, Yan, Y, Ruan, X, Warren, B, Lü, X, Li, X, Yao, Y, Huang, X, Yang, H & Xie, S 2021, 'Leaf wax and Sr-Nd isotope evidence for high-latitude dust input to the central South China sea and its implication for fertilization', *Geophysical Research Letters*, vol. 48, no. 11, e2020GL091853. <https://doi.org/10.1029/2020gl091853>

[Link to publication on Research at Birmingham portal](#)

Publisher Rights Statement:

An edited version of this paper was published by AGU. Copyright © 2021 American Geophysical Union.

Yang, Y., Bendle, J. A., Pancost, R. D., Yan, Y., Ruan, X., Warren, B., et al. (2021). Leaf wax and Sr-Nd isotope evidence for high-latitude dust input to the central South China Sea and its implication for fertilization. *Geophysical Research Letters*, 48, e2020GL091853. <https://doi.org/10.1029/2020GL091853>

General rights

Unless a licence is specified above, all rights (including copyright and moral rights) in this document are retained by the authors and/or the copyright holders. The express permission of the copyright holder must be obtained for any use of this material other than for purposes permitted by law.

- Users may freely distribute the URL that is used to identify this publication.
- Users may download and/or print one copy of the publication from the University of Birmingham research portal for the purpose of private study or non-commercial research.
- User may use extracts from the document in line with the concept of 'fair dealing' under the Copyright, Designs and Patents Act 1988 (?)
- Users may not further distribute the material nor use it for the purposes of commercial gain.

Where a licence is displayed above, please note the terms and conditions of the licence govern your use of this document.

When citing, please reference the published version.

Take down policy

While the University of Birmingham exercises care and attention in making items available there are rare occasions when an item has been uploaded in error or has been deemed to be commercially or otherwise sensitive.

If you believe that this is the case for this document, please contact UBIRA@lists.bham.ac.uk providing details and we will remove access to the work immediately and investigate.

1 **Leaf wax and Sr-Nd isotope evidence for high latitude dust input to the central South China Sea**
2 **and its implication for fertilization**

3
4 Yi Yang¹, James A. Bendle², Richard D. Pancost^{3,4}, Yan Yan⁵, Xiaoyan Ruan¹, Bridget Warren², Xiaoxia
5 Lü¹, Xuejie Li⁶, Yongjian Yao⁶, Xianyu Huang¹, Huan Yang¹, Shucheng Xie^{1,*}

6
7 ¹ State Key Laboratory of Biogeology and Environmental Geology, School of Earth Sciences, China
8 University of Geosciences, Wuhan 430074, China;

9 ² School of Geography, Earth and Environmental Sciences, University of Birmingham, Birmingham,
10 B15 2TT, UK;

11 ³ Organic Geochemistry Unit, School of Earth Sciences, School of Chemistry, University of Bristol,
12 Cantock's Close, Bristol BS8 1RJ, UK;

13 ⁴ University of Bristol Cabot Institute for the Environment, University of Bristol, Bristol BS8 1UJ;

14 ⁵ CAS Key Laboratory of Marginal Sea Geology, Guangzhou Institute of Geochemistry,
15 Chinese Academy of Sciences, Guangzhou, 510640, China;

16 ⁶ Guangzhou Marine Geological Survey, Ministry of Land and Resources, Guangzhou 510075, China

17 *Corresponding author: xiecug@163.com (S. Xie).

18
19 **Key Points:**

- 20 1. High concentrations of leaf-wax *n*-alkanes are measured in the South China Sea central basin
- 21 2. *n*-Alkane carbon preference index and hydrogen isotopic composition trace aeolian dust deposition from
22 higher latitudes to the central basin
- 23 3. Aeolian dust may play a significant role in regulating deposition of terrestrial organic matter in the
24 central South China Sea.

Formatted: Font: Times

Formatted: Font: Times

27 **Abstract**

28 Recent time-series from sediment traps show abnormally high chlorophyll-*a* concentrations and
29 primary productivity in the oligotrophic central South China Sea (SCS), especially during wintertime.
30 Here we present new insights from compound-specific hydrogen isotopic analysis of leaf wax *n*-alkanes
31 and Sr-Nd isotopes extracted from four basin-wide surface sediment transects. We find that the deepest
32 surface sediments in the central basin contain the most depleted *n*-alkane hydrogen isotopes, which is
33 suggestive of inputs from higher latitude soils in northern China. This is further supported by Sr-Nd
34 isotopes of the same surface sediments. We propose that aeolian dust is transported by the winter
35 monsoon and fertilizes the phytoplankton bloom in the central SCS. This process may have been
36 enhanced during glacial periods due to a stronger winter monsoon, driving both vertical mixing and
37 dust transport to the central basin.

38

39 *Keywords:* *n*-alkane, leaf wax, carbon and hydrogen isotopes, aeolian dust, Sr-Nd isotopes, South China
40 Sea

41

42

43 **Plain Language Summary:**

44 Recent studies observe abnormally high winter primary productivity and nitrate concentrations
45 in the surface waters of the central South China Sea. However, this is a nutrient limited region of the
46 ocean, so the drivers of this primary productivity are unclear. Here we analyze leaf wax carbon and
47 hydrogen isotopes, and Sr-Nd isotopes, at four shallow to deep water sediment transects to trace the
48 sources of dust and organic matter in the sediments of the central basin. Our results suggest the central
49 basin sediments receive significant terrestrial inputs of dust and nutrients from northern Asia via long-
50 range aeolian transport (during the winter monsoon). These results give new insights to terrestrial-
51 marine connections and the carbon cycle of the SCS. This process maybe a significant carbon sink in
52 the present-day and during the past.

53

54 **1. Introduction**

55 The marine biological pump plays an important role in manipulating glacial-interglacial
56 atmospheric CO₂, with the majority of carbon uptake apparently occurring in high latitude oceans such
57 as the Southern Ocean and subarctic Pacific (Brunelle et al., 2010; Martínez-García et al., 2014).
58 Recently, Buchanan et al. (2019) used a global marine biogeochemical model to show that the low
59 latitude ocean could be as important as high latitude locations for regulating atmospheric CO₂ during
60 glacial periods, due to Fe-induced stimulation of dinitrogen (N₂) fixation, strengthening the biological
61 pump, and ultimately causing CO₂ drawdown during glacial periods. This modelling work is consistent
62 with observations from ocean sediments cores that large quantities of sediments enriched in organic
63 carbon are preserved in continental seas and basins along continental margins at low latitudes (Berner,
64 1982; Hedges and Keil, 1995), suggesting an important role in the global carbon cycle (e.g., Dai et al.,
65 2013; Liu et al., 2010).

66 The South China Sea (SCS) is the largest marginal sea of the Pacific Ocean. It receives more than
67 700 million metric tons of fluvial sediments annually from surrounding rivers (Liu and Stattegger, 2014).
68 However, recent evidence highlights anomalously high phytoplankton distributions in the central SCS
69 where fluvial input is usually considered to be insignificant (Ma et al., 2013), indicating the central SCS
70 could be a significant carbon sink (Hung et al., 2020). In particular, satellite observations show
71 phytoplankton blooms, indicated by anomalously high concentrations of Chlorophyll-a, in the central

72 SCS during winter seasons (Ma et al., 2013; Ma et al., 2019). Export production from phytoplankton
73 blooms contributes a major source of organic matter (OM) to sediments. Sinking particle fluxes
74 including particulate organic matter (POM), calcium carbonate (CaCO₃), opal, and lithogenic matter
75 from long-term sediment traps show increased transportation and accumulation of biogenic materials
76 during the winter, within the central basin, compared with northern shallower traps (Li et al., 2017; Ma
77 et al., 2019; Priyadarshani et al., 2019; Zhang et al., 2019). Several 'bottom-up' driving mechanisms of
78 this phenomenon have been proposed, including the intrusion of Kuroshio surface waters (Hung et al.,
79 2007) and mesoscale eddies (Li et al., 2017) during the winter. However, the upwelling events induced
80 by Kuroshio intrusions and meso-scale eddies only account for about 20% of total deposition observed
81 in sediment traps between July 2012 and April 2013 (Zhang et al., 2019). Consequently, modern
82 observations of enhanced winter primary productivity in the central SCS requires an additional
83 mechanism for nutrient delivery.

84 One such potential driving mechanism is the 'top-down' delivery of dust, loaded with nutrients,
85 from higher latitudes by the East Asian Winter Monsoon (EAWM), which would stimulate nitrogen
86 fixation and the biological pump. Tracers for aeolian dust in marine sediments include minerals (Blank
87 et al., 1985; Liu et al., 2015), chemical components (Mcgee et al., 2016; Uematsu et al., 1983) and
88 terrestrial organics (Bendle et al., 2007; Bendle et al., 2006; Boreddy et al., 2017). Clay minerals and
89 grain sizes as well as chemical components have been discussed as possible input tracers for the SCS
90 (Boulay et al., 2007; Liu et al., 2016), but the mixed signal of the fluvial input, deep water current
91 transportation through Luzon strait, and/or the aeolian dust has made it difficult to confidently appoint
92 the sources of sediments to the central SCS.

93 The molecular and isotopic composition of leaf wax *n*-alkanes in aerosols has been widely used to
94 evaluate sources and pathways of airborne dust (Bendle et al., 2007; Ohkouchi et al., 1997; Schefuß et
95 al., 2003). For example, the carbon isotopic composition of plant wax *n*-alkanes has been used to map
96 the distribution of C₃/C₄ plants in source regions, and to decipher variations in vegetation in the
97 sediment record throughout the Quaternary (Jia et al., 2012; Li et al., 2015). Moreover, the δ²H values
98 of modern leaf wax *n*-alkanes are well correlated with the δ²H of meteoric water at latitudinal scales
99 (Rao et al., 2009) and are increasingly used in palaeohydrological reconstructions (Huang et al., 2018;
100 Thomas et al., 2014). The δ²H values and carbon preference indices (CPIs; ratio of odd-to-even chained
101 *n*-alkanes) of plant wax *n*-alkanes in East China surface soils exhibit a strong dependence on latitude

102 and the meteoric $\delta^2\text{H}$ line (Rao et al., 2009). The SCS region is strongly influenced by the East Asian
103 Monsoon, but whether the $\delta^2\text{H}$ values of *n*-alkanes from surface sediments can be used to constrain
104 sediment sources in the deep basin, which sits beyond the reach of most fluvial inputs, is still unknown.

105 We argue that the SCS represents a valuable research opportunity: local fluvial inputs are largely
106 captured on the continental shelf, whilst the middle of central basin (>4000m) sits beyond the reach of
107 most fluvial inputs. Thus, the deep SCS may capture a broad regional signal of aeolian dust inputs
108 (relatively uncontaminated by fluvial or biogenic factors) from a position proximal to the Asian
109 continent. We conduct a basin-wide survey of leaf wax molecular and isotopic distributions and
110 radiogenic Sr-Nd isotopes in the surface sediments of the SCS, and contrast this data with observations
111 and sedimentary of plankton groups in the SCS. This synthesis leads us to infer an increasing biological
112 pump for the anomalous wintertime phytoplankton bloom in the SCS on glacial-interglacial timescales.

113

114 2. Samples and Methods

115 2.1 Sampling sites

116 A total of 62 surface sediment samples were collected from the SCS (Fig. 1), with water depths
117 ranging from 30 to 4405m. The sampling transect therefore allows a comparison of the preservation of
118 terrestrial organic matter between shallow and deep-water sediments. The samples were collected using
119 a deep-sea sediment grab sampler or a box corer (0-5cm) and stored at -20°C prior to analysis.

120 2.2 TOC and Sr-Nd isotopic compositions analysis

121 For the TOC analysis, 1 gram sediment was decalcified with 2M HCl at room temperature for 24h,
122 then rinsed with pure water until pH = 7. Samples were freeze dried and transferred into tin capsules,
123 then analyzed by Elemental Analyzer. For the Sr-Nd isotopes analysis, 20 samples were digested in
124 Teflon bombs with mixed agents of double distilled HNO_3 and HF acid at 190 °C for 48h. Then, samples
125 were detected using a Triton T1 thermal ionization mass spectrometer (TIMS) and a Neptune Plus multi-
126 collector ICP-MS. The measured $^{143}\text{N}/^{144}\text{Nd}$ and $^{87}\text{Sr}/^{86}\text{Sr}$ ratios were normalized to $^{146}\text{Nd}/^{144}\text{Nd} =$
127 0.7219 and $^{86}\text{Sr}/^{88}\text{Sr} = 0.1194$, respectively. During the analysis, BCR-2 standard gave $^{87}\text{Sr}/^{86}\text{Sr} =$
128 0.704989 ± 8 (2σ) and $^{143}\text{N}/^{144}\text{Nd} = 0.512644 \pm 2$ (2σ). Nd results are calculated as $\epsilon\text{Nd}(0) =$
129 $[(^{143}\text{N}/^{144}\text{Nd})/0.512638] - 1 \times 10000$, using the chondritic uniform reservoir value given by Jacobsen
130 and Wasserburg (1980).

131 2.3 Lipid extraction and analysis.

132 Samples were freeze dried and homogenized with a pestle and mortar, then subjected to a
133 methodology modified from Yang et al. (2014). Samples were ultrasonically extracted with an azeotrope
134 of dichloromethane: MeOH (v/v 9:1) 5 times. All extracts were combined and collected after
135 centrifugation. The combined extracts were concentrated to 1-2 mL using rotary evaporation and dried
136 under a flow of N₂ gas. The total lipid extract was fractionated with *n*-hexane and MeOH into an apolar
137 fraction (containing the *n*-alkanes) and a polar fraction.

138 *n*-Alkanes were detected and identified by an Agilent 7890 gas chromatograph and 5975A mass
139 spectrometer (GC-MS) equipped with a DB-5MS capillary column (60m × 0.25mm × 0.25μm). The
140 alkane fraction was injected at a programmed temperature ramp of 3 °C/min⁻¹ from 70 to 300 °C and
141 held at 300 °C for 30 min. Relative compound abundances were calculated by comparing corresponding
142 MS (TIC) peak areas with internal standards of known concentration. Stable carbon and hydrogen
143 isotope compositions of individual *n*-alkanes were determined followed the program of Huang et al.
144 (2014) using a Finnigan Trace GC instrument attached to a Finnigan Delta Plus XP isotope ratio mass
145 spectrometer. Duplicate analyses were used to confirm that the standard deviations of leaf wax carbon
146 and hydrogen isotope determinations were better than ± 0.5‰ and 5‰ respectively. The δ¹³C and δ²H
147 values are reported in the delta notation (‰) relative to Vienna Pee Dee Belemnite (VPDB) and Vienna
148 Standard Mean Ocean Water (VSMOW), respectively.

149

150 **3. Results**

151 3.1 TOC and Sr-Nd isotope compositions

152 TOC values range from 0.12% to 0.82% (average 0.43%) in the SCS, and C/N values vary from
153 1.8 to 8.7 (average 6.3). Both TOC and C/N decrease with distance offshore, with high values in the
154 northern SCS, representing the higher organic matter deposits from fluvial inputs. However, in the
155 central basin, the TOC and C/N show an increase, with values comparable to those of the northern SCS
156 (Fig. 2A), suggesting a distinct source of terrestrial organic matter.

157 The ⁸⁷Sr/⁸⁶Sr and ¹⁴³Nd/¹⁴⁴Nd ratios range from 0.709161 to 0.712215 (average 0.712125) and from
158 0.512058 to 0.512425 (average 0.512154), respectively. εNd(0) values range from -11.31 to -4.15
159 (average -9.45). These values are consistent with previously published data of surface sediments from

160 the SCS (Liu et al., 2015, and references therein). Three samples from the northern and eastern SCS
161 with the highest $\epsilon\text{Nd}(0)$ (-6 to -4) derived from Luzon island (Liu et al., 2015).

162 3.2 Leaf wax molecular and isotopes distributions

163 The surface sediments contain *n*-alkanes characterized by a high odd-over-even carbon number
164 ranging in carbon number from C_{16} to C_{35} , with C_{31} dominant (Fig. S1). This is a clear signature of
165 terrestrial higher plant origin (Bush and McInerney, 2013; Eglinton and Hamilton, 1967). The
166 concentrations of total long chain *n*-alkanes show large variations, with anomalously high
167 concentrations in the deep central basin (Fig. 2B). CPI is typically around 2 in shallow surface sediments,
168 but it increases abruptly to 8 in the deepest basin (Fig. 2C). Concentrations of long chain diols (LCDs)
169 (algal biomarkers) range from 0.1 to 32.7 mg/g TOC dry sediments (Fig. 2D; Yang et al., 2020). It is
170 notable that both *n*-alkanes and planktonic LCDs comprise an enhanced proportion of the total organic
171 carbon (TOC) in the surface sediments deposited in the central basin, with TOC-normalized
172 concentrations up to three orders of magnitude higher in deep sediments than in shallow sediments (Fig.
173 3A-B).

174 Our *n*-alkane $\delta^{13}\text{C}$ values shift from -29 to -31‰ from the northeastern coast to the central basin
175 (Fig. 2E-F). The values in the deep central basin are similar to the northern SCS, and are highly variable
176 (Fig. 3E). *n*-Alkane $\delta^2\text{H}$ values vary from -140 to -160‰ in the northern SCS (Fig. 2G-H), but are
177 depleted in the deep central basin, with minimum values around -200‰. The lowest values (-190 to -
178 200 ‰) are distinct from the values observed in both Southern China catchment soils and the shallow
179 sediments (Fig. 1, Pelejero et al., 2003; Rao et al., 2009).

180

181 4. Discussion

182 4.1 Sources of surface sediments in the central SCS

183 The Sr-Nd isotopes from SCS surface sediments and surrounding fluvial drainage systems have
184 been well studied and were used to identify the sediment source provinces (Liu et al., 2016 and
185 references therein). Three samples from the northern and eastern SCS have a more positive $\epsilon\text{Nd}(0)$
186 falling within the variation range of the Luzon island (Liu et al., 2016), indicating the possible influence
187 of northern Luzon Arc material. The surrounding fluvial inputs have higher values of $^{87}\text{Sr}/^{86}\text{Sr}$ (>7.2,
188 Liu et al., 2016), which are distinguishable from our deep-water sediments, except for two samples
189 from the Red River. However, the clay mineral assemblages showed limited influence of the Red River

Commented [YY1]: 这后面部分想要去阐述吕宋岛弧和河流输入与深海盆之间的差异

190 on the SCS central basin (Liu et al., 2016). Our data shows that the more positive $\epsilon\text{Nd}(0)$ and lower
191 $^{87}\text{Sr}/^{86}\text{Sr}$ isotopes from the central basin sediments are not consistent with, and thus may not originate
192 from the surrounding fluvial drainage systems.

193 Instead, the $^{87}\text{Sr}/^{86}\text{Sr}$ and $\epsilon\text{Nd}(0)$ isotopes from the central basin are consistent with Asian dust
194 regions, suggesting a source relationship (Fig. 4A). This result is in line with the geochemical analyses
195 of sediments from Yongxing island in the SCS, which received significant high-latitude Asian aeolian
196 dust inputs (Liu et al., 2014). Grain size of the sediments might exert an impact on the Sr-Nd isotopes
197 as the Sr isotopic compositions are known to be strongly affected by the weathering, transportation and
198 deposition (Chen et al., 2007). The grain size of the sediments ranges from 0-400 μm (average medium
199 diameter $>5 \mu\text{m}$) in the northern and eastern SCS, but from 0-40 μm (average medium diameter $\sim 3\mu\text{m}$)
200 in the central SCS basin. Comparison of the grain size fractions suggests the Asian dust ($<5 \mu\text{m}$) falling
201 in the range of the SCS central basin is mainly contributed by the isotopic region B (i.e., the northern
202 margin of Tibetan Plateau) and C (i.e., the Ordos Plateau) (Fig. 4B). A calculation based on a simple
203 mass balance suggests 1:4 for the relative contribution of the isotopic regions B and C to the SCS central
204 basin (Fig. 4B).

205 *n*-Alkane CPIs of ~ 2 are consistent with those previously observed in shallow sediments from the
206 northern SCS (about 1.4 to 2.9 from Xu et al., 2014), and somewhat lower than those from surrounding
207 surface soils in Southern China (ca. 4, Rao et al., 2009; Luo et al., 2012), as well as northern SCS
208 Holocene sediments (ca. 2.3, Pelejero, 2003). Lower CPIs in marine sediments than in source catchment
209 soils suggest microbial degradation during riverine transportation (Ganeshram et al., 2011; Sun et al.,
210 2005). However, in the deepest SCS sediments, CPIs >3 are observed (Fig. 3C), with the highest CPI
211 measured approaching 8. Such high values are not observed in any of the shallow water settings
212 (Pelejero, 2003; Xu et al., 2014), suggesting that the terrestrial organic matter observed in this deep
213 basin setting is unlikely to be of riverine origin. CPIs of surface soils in eastern and northern China
214 show a strong relationship with latitude, with elevated values (> 5) observed in higher latitudes (Rao et
215 al., 2009). This high latitude CPI signature transported from the Asian dust area is also observed in the
216 deep-sea surface sediments collected from the Central Pacific (Ohkouchi et al., 1997). Comparison of
217 CPI values from SCS surface sediments with latitudinal soil profiles (Fig. S2), highlights that the high
218 CPI values (ca. 8) in the deep basin match source locations at mid-high latitudes (about 40°N) (Fig.
219 4C), where the loess plateau (with average CPI at 12.3; Liu and Huang, 2005; Luo et al., 2012) and

220 Gobi desert are located. Although *n*-alkane CPI covaries with various different environmental factors
221 (latitude, aridity and vegetation types) globally (Luo et al., 2012), latitude is still significant and
222 correlates broadly with CPI values (Fig. S2), with higher CPI in high latitudes. We propose the
223 distinctive CPI signature of the deepest SCS records are related to enhanced terrestrial organic matter
224 contributions via aeolian dust transported directly from vegetation or soils (Chikaraishi and Naraoka,
225 2003; Ning et al., 2005).

226 *n*-Alkane $\delta^2\text{H}$ values in East China surface soils also exhibit a strong dependence on latitude, with
227 lower values occurring at higher latitudes (Fig. 4D) (Rao et al., 2009). The $\delta^2\text{H}$ of southern Chinese
228 surface soils are around -160‰, consistent with northern SCS surface sediment values. However, the
229 $\delta^2\text{H}$ values in the central basin are more depleted and closer to higher latitude soil values (according to
230 the linear correlation between $\delta^2\text{H}$ and latitude (Fig. 4D)), supporting the above suggestion that *n*-
231 alkanes deposited in the central SCS are sourced from high-latitude dust inputs. The trend with water
232 depth for *n*-alkane $\delta^{13}\text{C}$ values in the SCS is more variable than for $\delta^2\text{H}$. *n*-Alkane $\delta^{13}\text{C}$ is used to trace
233 the relative contribution of C_3 and C_4 plant types. The *n*-alkane $\delta^{13}\text{C}$ through the SCS thus likely records
234 the C_3/C_4 plant signal in terrestrial inputs to the SCS. The *n*-alkane $\delta^{13}\text{C}$ in the SCS surface sediments
235 is consistent with inputs from a diverse and mixed distribution of C_3 and C_4 plants extending from
236 Southeast Asia throughout mainland China (Still et al., 2009). Thus in this context $\delta^{13}\text{C}$ values are not
237 as diagnostic as the corresponding $\delta^2\text{H}$ values and CPIs for indicative of source regions.

238 Comparison of *n*-alkane $\delta^2\text{H}$ and CPI data from the central basin with the available soil *n*-alkane
239 data (this study and Rao et al., 2009, Fig. 4C-D), suggests significant soil inputs from $>40^\circ\text{N}$, ca.
240 2000km to the north of the SCS region. High latitude arid and semi-arid regions in China and Asia,
241 especially the Taklimakan desert (located at ca. 35 to 45°N), are major sources of atmospheric dust in
242 the Northern Hemisphere (add ref). During the winter monsoon, decreased winter precipitation allows
243 more aeolian dust transport to the SCS, while only minimal inputs of entrained dust occurs during the
244 summer monsoon, due to heavy summer precipitation and rainout of dust closer to source regions
245 (Boulay et al., 2003; Tian et al., 2005). We conducted a seasonal back trajectory air masses model which
246 simulated the seasonal organic matter transport pathway to the central SCS (13°N , 115°E). The result
247 shows a larger amount of dust transport from central Asia during the winter season compared to the
248 summer season (Fig. S3), which is consistent with the results from Yongxin island (Xiao et al., 2017).
249 Our *n*-alkane isotopic signatures (low $\delta^2\text{H}$ values) are consistent with enhanced delivery of aeolian dust

Formatted: Font color: Red

250 to the central SCS by the winter monsoon. The lipid profile results agree with the $^{87}\text{Sr}/^{86}\text{Sr}$ and $\epsilon\text{Nd}(0)$
251 evidence, both confirm dust inputs from high latitude Asian source regions to the deep central basin of
252 the SCS.

253

254 4.2 Enhanced Aeolian dust input to the SCS central basin and its implications

255 Our results show both terrestrial leaf wax *n*-alkane and LCD concentrations increase in the central
256 basin compared to northern SCS. Trace metal (Sr-Nd) isotopes from the same stations also constrain
257 the original sources to predominantly mid-latitude Asian deserts (Fig. 4A-B). It is interesting to note
258 that time-series sediment trap data from the SCS quantified the effects of the different processes on
259 sinking particle fluxes, and highlighted that the northeast winter monsoon and associated aerosol
260 deposition events played key roles in sediment deposition during the winter monsoon period (58.7%,
261 Zhang et al., 2019, from October to April). Consequently, our investigations on surface sediments - and
262 the reported time-series trap data - both indicate an important contribution of Asian dust to the SCS
263 central basin.

264 Of significance is that Asian dust inputs are elevated during the winter season due to the occurrence
265 of the enhanced Winter Asian Winter Monsoon. This is of importance for connections to the carbon-
266 cycle, via processes such as fertilization of phytoplankton and the rapid deposition of organic matter.
267 Both *n*-alkane and LCD concentrations are elevated in the surface sediments of the central basin
268 compared with the northern SCS, and high *n*-alkane CPI values indicate relatively fresh organic matter
269 deposition to the deepest water sites in the central SCS. These results are consistent with enhanced
270 satellite Chl-*a* concentration and organic matter collected from time-series sediment traps in the central
271 basin (Li et al., 2017; Ma et al., 2019; Priyadarshani et al., 2019; Zhang et al., 2019). Seasonal time-
272 series data analysis shows higher OM deposition during the winter season when EAWM conditions
273 prevail.

274 A “bottom-up” mechanism driving phytoplankton blooms and biomass in the marginal, stratified
275 regions of the SCS has been well characterised (Chen, 2005; Tang et al., 1999; Li et al., 2017). During
276 the winter season, the frequency of cold meso-scale eddies increases in the central SCS, which drives
277 nutrient-rich subsurface waters to the surface and stimulates phytoplankton blooms in the oligotrophic
278 SCS central basin (Chen, 2005; Tang et al., 1999). Coupled with the meso-scale eddies during winter
279 season, vertical mixing in the upper water column is strongest in the central basin, and is about four

280 times deeper in winter than is seen in the rest of the year (Lu et al., 2020; Qu, 2001). Increased vertical
281 mixing drives higher concentrations of nitrate to the surface layer and fertilizes the phytoplankton
282 bloom in the central basin. This mechanism explains the higher nitrate concentration and primary
283 production in the central basin compared to the northern SCS observed in satellite data. Logically,
284 increased carbon export to the SCS during the winter monsoon will lead to the deposition of an outsized
285 proportion of these sediments during that time interval. This bottom-up mechanism successfully
286 explains the abnormal high chl-a and high OC fluxes at the central basin, but cannot reconcile the high
287 terrestrial sourced *n*-alkane distribution in the central SCS.

288 High concentrations of high CPI *n*-alkanes which are depleted in $\delta^2\text{H}$ demonstrate the importance
289 of aeolian dust deposition in the transport of organic matter to the central SCS (Fig. 4C-D). We propose
290 a “top-down” mechanism could be essential to explain the observed distributions of *n*-alkane and long
291 chain diols in the surface sediments of the central SCS basin. Windborne dust particles containing both
292 lithogenic material and land-derived lipids are significant in the rapid transfer of newly fixed organic
293 carbon from the sea surface to the bottom (Ittekkot et al., 1992). The incorporation of minerals into
294 biologically formed aggregates ensures the rapid deposition of fresh *n*-alkanes with higher CPI in the
295 central basin. Meanwhile, modern observation studies suggest Asian dust events could enhance
296 phytoplankton growth and primary production in Chinese marginal seas (Tan et al., 2011; Tan et al.,
297 2012; Wang et al., 2012), which further supports evidence from TOC, carbonate, microfossil and lipid
298 profiles studies (Thunell et al., 1992; Huang et al., 1997a; Huang et al., 1997b; Shiao et al., 2008; Ren
299 et al., 2017). Long time *in situ* studies revealed aerosol deposition of dissolved inorganic nitrogen to
300 the SCS, especially in the basin area, was approximately 20% on average (Kim et al., 2014; Shen et al.,
301 2020; Gao et al., 2020). This atmospheric N deposition could support the primary production in the
302 oligotrophic water of the SCS, which is characterized by limited nitrate.

303 Dust regulated iron supply might stimulate the nitrogen fixation, and is crucial in linking the
304 biological cycling of iron to the assimilation of major nutrients and carbon fixation (Tagliabue et al.,
305 2017). A recent model study shows Fe-induced stimulation of N_2 fixation pathways could drive a
306 considerable uptake of carbon dioxide in low latitude oceans during dusty glacial conditions (Buchanan
307 et al., 2019). Gaye et al. (2009) proposed the N_2 fixation contributed up to 20% to settling particle
308 nitrogen in the deep SCS, about twice the estimated contribution in the northern SCS (Kao et al., 2012;
309 Wong et al., 2007; Zhang et al., 2015). However, both foraminifera-bound nitrogen isotope records and

Formatted: Font: Italic

Commented [MOU2]: Which basin?

Commented [MOU3]: 20% of what? 20% of total annual flux?

310 ammonia oxidizing archaea records from the SCS (Ren et al., 2017; Dong et al., 2019) reconstruct lower
311 N₂ fixation rates during glacial periods, despite the observed increase in dust deposition and productivity.
312 Thus the role of Fe fertilization in regulating the SCS carbon and nitrogen cycles requires further
313 investigation.

314 In summary our evidence from terrestrial leaf wax (*n*-alkane) and marine phytoplankton (LCDs)
315 biomarkers is consistent with sediment trap time-series data (ref) and suggests a role for aerosol dust
316 deposition in the winter phytoplankton blooms as observed by satellite in the central basin of the SCS
317 (Ma et al., 2013). During the winter monsoon it appears that dust supplied from higher latitudes and
318 vertical oceanic mixing supplies higher nutrients and triggers new production in the central SCS. Our
319 results are also important for paleoclimate reconstructions, as this process would be expected to deliver
320 enhanced supplies of terrestrial, nutrient bearing, dust during the glacial periods (Shiau et al., 2008; Ren
321 et al., 2017). However, precise mechanisms and the relative importance of, for example, Fe fertilization
322 in currently ambiguous. Thus more work, including *in-situ* monitoring in the central basin and model
323 simulations are required to elucidate mechanisms, quantify fluxes and understand the importance of
324 dust deposition at the air-water interface in low latitude marginal seas.

Formatted: Font: Italic

325

326 5. Conclusions

327 Multiple lines of evidence based on high *n*-alkane CPI, depleted δ²H, and Sr-Nd isotope values
328 in surface sediments highlight the transport and deposition of dust from high latitude regions to the
329 central SCS basin. We conclude aeolian dust from northern China is transported by the East Asia Winter
330 Monsoon and contributes (along with vertical mixing of nutrients) to the triggering of the winter
331 phytoplankton in the central SCS. The intimate biotic-abiotic association triggered by dust supply could
332 accelerate the organic deposition rate and thus has implications for the biological pump. Our results
333 shows that nitrogen fixation in the marginal SCS central basin could be as important as vertical mixing,
334 both in increasing primary production and for high sediment deposition rates. Thus the SCS central
335 basin could be a significant, but hitherto overlooked, carbon sink during the present day and glacial
336 periods, which merits further investigation.

Formatted: Font: Italic

337

338

339

340 **Acknowledgements**

341 We thank the Editors Dr. Angelique White, Dr. Sarah Feakins and two anonymous reviewers for their
342 constructive comment to improve the quality of this manuscript. The work was supported by the State Key
343 R&D Program of China (Grant No.2016YFA0601100), the National Natural Science Foundation of China
344 (Grant No. 41821001 and 41830319), Guangzhou Marine Geological Survey (Grant No. [2015] GZH01-02-
345 6). We thank the China Scholarship Council (CSC) (Grant No. xxxxx) for supporting Yang Yi's study visit
346 to the University of Birmingham

Formatted: Highlight

Formatted: Highlight

Formatted: Highlight

348 **Data Availability Statement**

349 All of the original data has been uploaded as supplemental material and will be deposited publicly to
350 the repository of Zenodo, once it is accepted for publishing. All the supporting data can be found in the cited
351 references (Rao et al., 2009; Luo et al., 2012; Liu et al., 2007; Pettke et al., 2000; Defant et al., 1990; Jiang
352 et al., 2013; Chen et al., 2007; Liu et al., 2014; Biscaye et al., 1997).

354 **References**

- 355 Bendle, J., Kawamura, K., Yamazaki, K., Niwai, T. (2007). Latitudinal distribution of terrestrial lipid biomarkers
356 and n-alkane compound-specific stable carbon isotope ratios in the atmosphere over the western Pacific and
357 Southern Ocean. *Geochimica et Cosmochimica Acta*, 71, 5934-5955.
- 358 Bendle, J.A., Kawamura, K., Yamazaki, K. (2006). Seasonal changes in stable carbon isotopic composition of n-
359 alkanes in the marine aerosols from the western North Pacific: Implications for the source and atmospheric
360 transport. *Geochimica et Cosmochimica Acta*, 70, 13-26.
- 361 Berner, R.A., (1982). Burial of organic carbon and pyrite sulfur in the modern ocean: its geochemical and
362 environmental significance. *American Journal of Science*, 282, 451-473.
- 363 Biscaye, P. E., Grousset, F. E., Revel, M., Van der Gaast, S., Zielinski, G. A., Vaars, A., Kukla, G. (1997). Asian
364 provenance of glacial dust (stage 2) in the Greenland Ice Sheet Project 2 ice core, Summit, Greenland. *Journal*
365 *of Geophysical Research: Oceans*, 102, 26765-26781.
- 366 Blank, M., Leinen, M., Prospero, J.M. (1985). Major
367 Asian aeolian inputs indicated by the mineralogy of aerosols and sediments in the western North Pacific.
Nature, 314, 84-86.
- 368 Boreddy, S.K.R., Haque, M.M., Kawamura, K. (2017). Long-term (2001–2012) trends of carbonaceous aerosols

369 from remote island in the western North Pacific: an outflow region of Asian pollutants and dust. *Atmospheric*
370 *Chemistry & Physics*, 1-21.

371 Boulay, S., Colin, C., Trentesaux, A., Clain, S., Liu, Z., Lauer-Leredde, C. (2007). Sedimentary responses to the
372 Pleistocene climatic variations recorded in the South China Sea. *Quaternary Research*, 68, 162-172.

373 Boulay, S., Colin, C., Trentesaux, A., Pluquet, F., Bertaux, J., Blamart, D., Buehring, C., Wang, P. (2003).
374 Mineralogy and sedimentology of Pleistocene sediment in the South China Sea (ODP Site 1144), Proceedings
375 of the ocean drilling program, scientific results, 1-21.

376 Brunelle, B.G., Sigman, D.M., Jaccard, S.L., Keigwin, L.D., Plessen, B., Schettler, G., Cook, M.S., Haug, G.H.
377 (2010). Glacial/interglacial changes in nutrient supply and stratification in the western subarctic North Pacific
378 since the penultimate glacial maximum. *Quaternary Science Reviews*, 29, 2579-2590.

379 Buchanan, P.J., Chase, Z., Matear, R.J., Phipps, S.J., Bindoff, N.L. (2019). Marine nitrogen fixers mediate a low
380 latitude pathway for atmospheric CO₂ drawdown. *Nature communications*, 10, 1-10.

381 Bush, R.T., McInerney, F.A. (2013). Leaf wax *n*-alkane distributions in and across modern plants: implications
382 for paleoecology and chemotaxonomy. *Geochimica et Cosmochimica Acta*, 117, 161-179.

383 Chen, J., Li, G., Yang, J., Rao, W., Lu, H., Balsam, W., Sun, Y., Ji, J. (2007). Nd and Sr isotopic characteristics of
384 Chinese deserts: implications for the provenances of Asian dust. *Geochimica et Cosmochimica Acta*, 71,
385 3904-3914.

386 Chen, Y.-l.L., (2005). Spatial and seasonal variations of nitrate-based new production and primary production in
387 the South China Sea. *Deep Sea Research Part I: Oceanographic Research Papers*, 52, 319-340.

388 Chikaraishi, Y., Naraoka, H. (2003). Compound-specific $\delta^{13}\text{C}$ analyses of *n*-alkanes extracted from terrestrial and
389 aquatic plants. *Phytochemistry*, 63, 361-371.

390 Dai, M., Cao, Z., Guo, X., Zhai, W., Liu, Z., Yin, Z., Xu, Y., Gan, J., Hu, J., Du, C. (2013). Why are some marginal
391 seas sources of atmospheric CO₂? *Geophysical Research Letters*, 40, 2154-2158.

392 Dong, Liang, Zhiyang Li, and Guodong Jia, (2019). Archaeal ammonia oxidation plays a part in late Quaternary
393 nitrogen cycling in the South China Sea." *Earth and Planetary Science Letters*, 509, 38-46.

394 Defant, M.J., Maury, R.C., Joron, J.-L., Feigenson, M.D., Leterrier, J., Bellon, H., Jacques, D., Richard, M. (1990).
395 The geochemistry and tectonic setting of the northern section of the Luzon arc (the Philippines and Taiwan).
396 *Tectonophysics*, 183, 187-205.

397 Eglinton, G., Hamilton, R.J. (1967). Leaf epicuticular waxes. *Science*, 156, 1322-1335.

398 Ganeshram, R.S., Bryant, C.L., Cisneros, L.M. (2011). Sources of *n*-alkanes in an urbanized estuary: Insights

399 from molecular distributions and compound-specific stable and radiocarbon isotopes. *Marine Chemistry*, 126,
400 239-249.

401 Gao, Y., Wang, L., Guo, X., Xu, Y. and Luo, L., (2020). Atmospheric wet and dry deposition of dissolved inorganic
402 nitrogen to the South China Sea. *Science China Earth Sciences*, 63(9), 1339-1352.

403 Gaye, B., Wiesner, M., Lahajnar, N. (2009). Nitrogen sources in the South China Sea, as discerned from stable
404 nitrogen isotopic ratios in rivers, sinking particles, and sediments. *Marine Chemistry* 114, 72-85.

405 Hedges, J.I., Keil, R.G. (1995). Sedimentary organic matter preservation: an assessment and speculative synthesis.
406 *Marine Chemistry*, 49, 81-115.

407 Huang, C. Y., P. M. Liew, M. Zhao, T. C. Chang, C. M. Kuo, M. T. Chen, C. H. Wang, and L. F. Zheng, (1997a):
408 Deep sea and lake records of the Southeast Asian paleomonsoons for the last 25 kyrs. *Earth and Planetary Science*
409 *Letters*, 146, 59-72.

410 Huang, C. Y., S. F. Wu, M. Zhao, M. T. Chen, C. H. Wang, X. Tu, and P. B. Yuan, (1997b): Surface ocean and
411 monsoon climate variability in the South China Sea since last glaciation. *Marine Micropaleontology*, 32, 71-
412 94. Huang, X., Pancost, R.D., Xue, J., Gu, Y., Evershed, R.P., Xie, S., (2018). Response of carbon cycle to drier
413 conditions in the mid-Holocene in central China. *Nature communications*, 9, 1-9

414 Huang, X., Xue, J., Meyers, P.A., Gong, L., Wang, X., Liu, Q., Qin, Y., Wang, H. (2014). Hydrologic influence
415 on the $\delta^{13}\text{C}$ variation in long chain n -alkanes in the Dajuhu peatland, central China. *Organic Geochemistry*,
416 69, 114-119.

417 Hung, J.-J., Wang, S.-M., Chen, Y.-L. (2007). Biogeochemical controls on distributions and fluxes of dissolved
418 and particulate organic carbon in the Northern South China Sea. *Deep Sea Research Part II: Topical Studies*
419 *in Oceanography*, 54, 1486-1503.

420 Hung, J.-J., Wang, Y.-J., Tseng, C.-M., Chen, Y.-L.L. (2020). Controlling mechanisms and cross linkages of
421 ecosystem metabolism and atmospheric CO₂ flux in the northern South China Sea. *Deep Sea Research Part*
422 *I: Oceanographic Research Papers*, 157, 103205.

423 Ittekkot, V., Haake, B., Bartsch, M., Nair, R.R. and Ramaswamy, V., (1992). Organic carbon removal in the sea:
424 the continental connection. *Geological Society, London, Special Publications*, 64(1), 167-176.

425 Jacobsen, S.B., Wasserburg, G. (1980). Sm-Nd isotopic evolution of chondrites. *Earth and Planetary Science*
426 *Letters*, 50, 139-155.

427 Jia, G., Li, Z., Peng, P.A., Zhou, L. (2012). Eolian n -alkane isotopic evidence from North Pacific for a Late
428 Miocene decline of C₄ plant in the arid Asian interior. *Earth and Planetary Science Letters*, 321, 32-40.

429 Jiang, F., Frank, M., Li, T., Chen, T.Y., Xu, Z., Li, A. (2013). Asian dust input in the western Philippine Sea:
430 Evidence from radiogenic Sr and Nd isotopes. *Geochemistry, Geophysics, Geosystems*, 14, 1538-1551.

431 Kao, S.J., Terence Yang, J.Y., Liu, K.K., Dai, M., Chou, W.C., Lin, H.L., Ren, H. (2012). Isotope constraints on
432 particulate nitrogen source and dynamics in the upper water column of the oligotrophic South China Sea.
433 *Global biogeochemical cycles*, 26,1-15.

434 Kim, T. W., Lee,K., Duce,R., Liss,P. (2014). Impact of atmospheric nitrogen deposition on phytoplankton
435 productivity in the South China Sea, *Geophysical Research Letters*, 41, 3156-3162.

436 Li, H., Wiesner, M.G., Chen, J., Ling, Z., Zhang, J., Ran, L. (2017). Long-term variation of mesopelagic biogenic
437 flux in the central South China Sea: Impact of monsoonal seasonality and mesoscale eddy. *Deep Sea*
438 *Research Part I: Oceanographic Research Papers*, 126, 62-72.

439 Li, L., Li, Q., Li, J., Wang, H., Dong, L., Huang, Y., Wang, P. (2015). A hydroclimate regime shift around 270 ka
440 in the western tropical Pacific inferred from a late Quaternary n -alkane chain-length record.
441 *Palaeogeography Palaeoclimatology Palaeoecology*, 427, 79-88.

442 Liu, K.-K., Atkinson, L., Quiñones, R., Talaue-McManus, L. (2010). Carbon and nutrient fluxes in continental
443 margins: a global synthesis. Springer Science & Business Media.

444 Liu, Q., Sun, Y., Qiang, X., Tada, R., Hu, P., Duan, Z., Jiang, Z., Liu, J., Su, K. (2015). Characterizing magnetic
445 mineral assemblages of surface sediments from major Asian dust sources and implications for the Chinese
446 loess magnetism. *Earth Planets and Space*, 67, 1-17.

447 Liu, W., Huang, Y., (2005). Compound specific D/H ratios and molecular distributions of higher plant leaf waxes
448 as novel paleoenvironmental indicators in the Chinese Loess Plateau. *Organic Geochemistry*, 36, 851-860.

449 Liu, Y., Sun, L., Zhou, X., Luo, Y., Huang, W., Yang, C., Wang, Y., Huang, T. (2014). A 1400-year terrigenous
450 dust record on a coral island in South China Sea. *Scientific Reports*, 4, 4994.

451 Liu, Z., Colin, C., Huang, W., Le, K.P., Tong, S., Chen, Z., Trentesaux, A. (2007). Climatic and tectonic controls
452 on weathering in south China and Indochina Peninsula: Clay mineralogical and geochemical investigations
453 from the Pearl, Red, and Mekong drainage basins. *Geochemistry, Geophysics, Geosystems*, 8, 1-18.

454 Liu, Z., Statterger, K. (2014). South China Sea fluvial sediments: an introduction preface. *Journal of Asian Earth*
455 *Sciences*, 79, 507-508.

456 Liu, Z., Zhao, Y., Colin, C., Statterger, K., Wiesner, M.G., Huh, C.A., Zhang, Y., Li, X., Sompongchaiyakul, P.,
457 You, C.F. (2016). Source-to-sink transport processes of fluvial sediments in the South China Sea. *Earth-*
458 *Science Reviews*, 153, 238-273.

459 Lu, Z., Gan, J., Dai, M., Zhao, X., Hui, C.R. (2020). Nutrient transport and dynamics in the South China Sea: A
460 modeling study. *Progress in Oceanography*, 102308.

461 Luo, P., Peng, P., Lü, H., Zheng, Z., Wang, X. (2012). Latitudinal variations of CPI values of long-chain *n*-alkanes
462 in surface soils: Evidence for CPI as a proxy of aridity. *Science China Earth Sciences*, 55, 1134-1146.

463 Ma, W., Chai, F., Xiu, P., Xue, H., Tian, J. (2013). Modeling the long-term variability of phytoplankton functional
464 groups and primary productivity in the South China Sea. *Journal of Oceanography*, 69, 527-544.

465 Ma, W., Xiu, P., Chai, F., Li, H. (2019). Seasonal variability of the carbon export in the central South China Sea.
466 *Ocean Dynamics*, 69, 955-966.

467 Martínez-García, A., Sigman, D.M., Ren, H., Anderson, R.F., Straub, M., Hodell, D.A., Jaccard, S.L., Eglinton,
468 T.I., Haug, G.H. (2014). Iron fertilization of the Subantarctic Ocean during the last ice age. *Science*, 343,
469 1347-1350.

470 Mcgee, D., Winckler, G., Borunda, A., Serno, S., Anderson, R.F., Recasens, C., Bory, A., Gaiero, D., Jaccard, S.L.,
471 Kaplan, M. (2016). Tracking eolian dust with helium and thorium: Impacts of grain size and provenance.
472 *Geochimica et Cosmochimica Acta*, 175, 47-67.

473 Ning, X., Chai, F., Xue, H., Cai, Y., Liu, C., Zhu, G., Shi, J. (2005). Physical-biological oceanographic coupling
474 influencing phytoplankton and primary production in the South China Sea. *Journal of Geophysical Research*
475 *Oceans* 110, 215-255.

476 Ohkouchi, N., Kawamura, K., Kawahata, H., Taira, A. (1997). Latitudinal distributions of terrestrial biomarkers
477 in the sediments from the Central Pacific. *Geochimica et Cosmochimica Acta*, 61, 1911-1918.

478 Pelejero, C. (2003). Terrigenous *n*-alkane input in the South China Sea: high-resolution records and surface
479 sediments. *Chemical Geology*, 200, 89-103.

480 Pettke, T., Halliday, A.N., Hall, C.M., Rea, D.K., 2000. Dust production and deposition in Asia and the north
481 Pacific Ocean over the past 12 Myr. *Earth and Planetary Science Letters* 178, 397-413.

482 Priyadarshani, W., Ran, L., Wiesner, M.G., Chen, J., Ling, Z., Yu, S., Ye, Y. (2019). Seasonal and interannual
483 variability of coccolithophore flux in the northern South China Sea. *Deep Sea Research Part I: Oceanographic Research Papers*, 145, 13-30.

484 Qu, T., (2001). Role of ocean dynamics in determining the mean seasonal cycle of the South China Sea surface
485 temperature. *Journal of Geophysical Research: Oceans*, 106, 6943-6955.

486 Rao, Z.G., Zhu, Z.Y., Jia, G.D., Henderson, A.C.G., Xue, Q., Wang, S.P. (2009). Compound specific δD values of
487 long chain *n*-alkanes derived from terrestrial higher plants are indicative of the δD of meteoric waters:

489 evidence from surface soils in eastern China. *Organic Geochemistry*, 40, 922-930.

490 Ren, H., Sigman, D.M., Martínez-García, A., Anderson, R.F., Chen, M.T., Ravelo, A.C., Straub, M., Wong, G.T.
491 and Haug, G.H., (2017). Impact of glacial/interglacial sea level change on the ocean nitrogen
492 cycle. *Proceedings of the National Academy of Sciences*, 114(33), 6759-6766.

493 Schefuß, E., Ratmeyer, V., Stuut, J.B.W., Jansen, J.H.F., Sinninghe Damsté, J.S. (2003). Carbon isotope analyses
494 of *n*-alkanes in dust from the lower atmosphere over the central eastern Atlantic. *Geochimica et*
495 *Cosmochimica Acta*, 67, 1757-1767.

496 Shen, C., Zhao, H., Chen, F. and Xiao, H., (2020). The Distribution of Aerosols and Their Impacts on Chlorophyll-
497 a Distribution in the South China Sea. *Journal of Geophysical Research: Biogeosciences*, 125(6).

498 Shiau, L.J., Yu, P.S., Wei, K.Y., Yamamoto, M., Lee, T.Q., Yu, E.F., Fang, T.H. and Chen, M.T., (2008). Sea Surface
499 Temperature, Productivity, and Terrestrial Flux Variations of the Southeastern South China Sea over the Past
500 800000 Years (IMAGES MD972142). *Terrestrial, Atmospheric & Oceanic Sciences*, 19(4).

501 Still, C.J., Berry, J.A., Collatz, G.J., Defries, R.S. (2009). ISLSCP II C4 Vegetation Percentage. ORNL Distributed
502 Active Archive Center, Oak Ridge, Tennessee, USA.

503 Sun, Y., Chen, Z., Xu, S., Cai, P. (2005). Stable carbon and hydrogen isotopic fractionation of individual *n*-alkanes
504 accompanying biodegradation: evidence from a group of progressively biodegraded oils. *Organic*
505 *Geochemistry*, 36, 225-238.

506 Tagliabue, A., Bowie, A.R., Boyd, P.W., Buck, K.N., Johnson, K.S., Saito, M.A. (2017). The integral role of iron
507 in ocean biogeochemistry. *Nature*, 543, 51-59.

508 Tang, D.-L., Ni, I.-H., Kester, D.R., Müller-Karger, F.E. (1999). Remote sensing observations of winter
509 phytoplankton blooms southwest of the Luzon Strait in the South China Sea. *Marine Ecology Progress Series*,
510 191, 43-51.

511 Tan, S.C.; Shi, G.Y.; Shi, J. H. (2011). Correlation of Asian dust with chlorophyll and primary productivity in
512 coastal seas of China during the period 1997 to 2008. *Journal of Geophysical Research*, 116, G02029.

513 Tan, S.C.; Shi, G. Y. (2012). The relationship between satellite-derived primary production and vertical mixing
514 and atmospheric inputs in the Yellow Sea cold water mass. *Continental Shelf Research*, 48,138–145.

515 Thomas, E.K., Clemens, S.C., Prell, W.L., Herbert, T.D., Huang, Y., Liu, Z., Sinninghe Damste, J.S., Sun, Y., Wen,
516 X. (2014). Temperature and leaf wax 2H records demonstrate seasonal and regional controls on Asian

Formatted: Indent: Left: 0 cm, Hanging: 2 ch, First line: -2 ch

517 monsoon proxies. *Geology*, 42, 1075-1078.

518 Tian, J., Wang, P., Chen, R., Cheng, X. (2005). Quaternary upper ocean thermal gradient variations in the South
519 China Sea: Implications for east Asian monsoon climate. *Paleoceanography*, 20, 1-8.

520 Thunell, R. C., Q. Miao, S. E. Calvert, and T. F. Pedersen, (1992). Glacial-Holocene biogenic sedimentation
521 patterns in the South China Sea: Productivity variations and surface water pCO₂. *Paleoceanography*, 7,
522 143-162.

523 Uematsu, M., Duce, R.A., Prospero, J.M., Chen, L., Merrill, J.T., Medonald, R.L. (1983). Transport of mineral
524 aerosol from Asia Over the North Pacific Ocean. *Journal of Geophysical Research Oceans*, 88, 5343-5352.

525 Wang, S.H.; Hsu, N.C.; Tsay, S.C.; Lin, N.H.; Sayer, A.M.; Huang, S.J.; Lau, W.K. M. (2012). Can Asian dust
526 trigger phytoplankton blooms in the oligotrophic northern South China Sea? *Geophysical Research Letters*,
527 39, L05811.

528 Wong, G.T., Tseng, C.-M., Wen, L.-S., Chung, S.-W. (2007). Nutrient dynamics and N-anomaly at the SEATS
529 station. *Deep Sea Research Part II: Topical Studies in Oceanography*, 54, 1528-1545.

530 Xu, W., Yan, W., Chen, Z., Chen, H., Huang, W., Lin, T. (2014). Organic matters and lipid biomarkers in surface
531 sediments from the northern South China Sea: Origins and transport. *Journal of Earth Science*, 25, 189-196.

532 Yang, H., Pancost, R.D., Dang, X., Zhou, X., Evershed, R.P., Xiao, G., Tang, C., Gao, L., Guo, Z., Xie, S. (2014).
533 Correlations between microbial tetraether lipids and environmental variables in Chinese soils: Optimizing
534 the paleo-reconstructions in semi-arid and arid regions. *Geochimica et Cosmochimica Acta*, 126, 49-69.

535 Yang, Y., Gao, C., Dang, X.Y., Ruan, X.Y., Lü, X.X., Xie, S.C., Li, X.J., Yao, Y.J., Yang, H. (2018). Assessing
536 hydroxylated isoprenoid GDGTs as a paleothermometer for the tropical South China Sea. *Organic*
537 *Geochemistry*, 115, 156-165.

538 Yang, Y., Ruan, X., Gao, C., Lü, X.X., Yang, H., Li, X., Yao, Y., Pearson, A. and Xie, S., (2020). Assessing the
539 applicability of the long-chain diol (LDI) temperature proxy in the high-temperature South China
540 Sea. *Organic Geochemistry*, 104017.

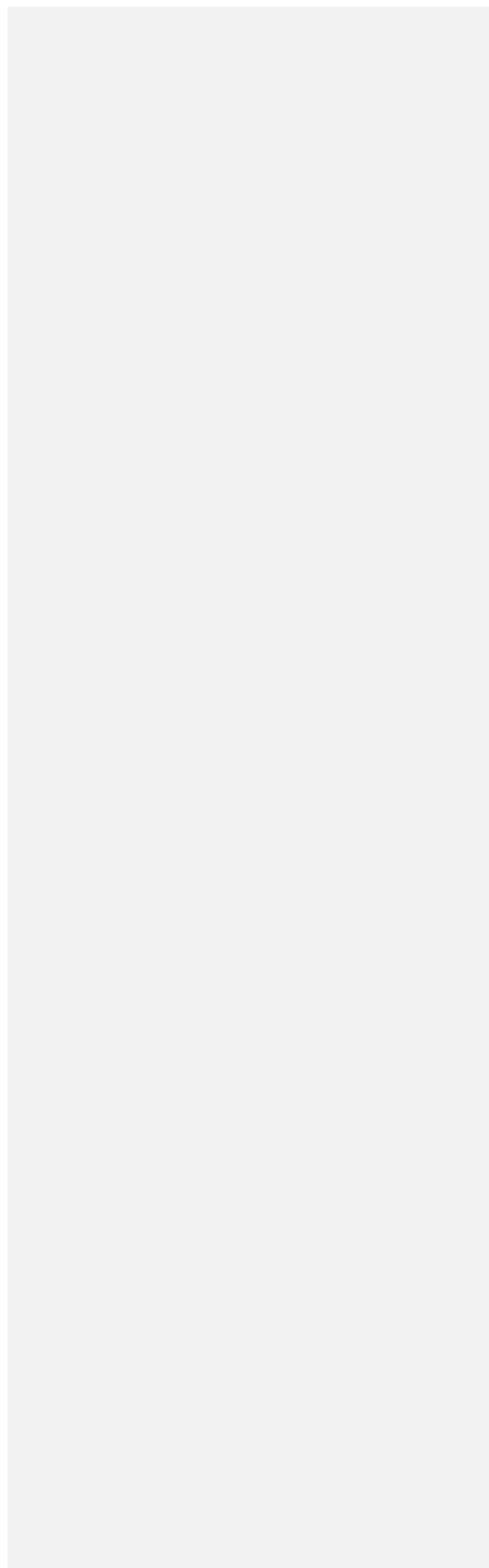
541 Zhang, J., Li, H., Xuan, J., Wu, Z., Yang, Z., Wiesner, M.G., Chen, J. (2019). Enhancement of mesopelagic sinking
542 particle fluxes due to upwelling, aerosol deposition, and monsoonal influences in the northwestern South
543 China Sea. *Journal of Geophysical Research: Oceans*, 124, 99-112.

544 Zhang, R., Chen, M., Yang, Q., Lin, Y., Mao, H., Qiu, Y., Tong, J., Lv, E., Yang, Z., Yang, W. (2015). Physical-
545 biological coupling of N₂ fixation in the northwestern South China Sea coastal upwelling during summer.

546 *Limnology and Oceanography*, 60, 1411-1425.

547

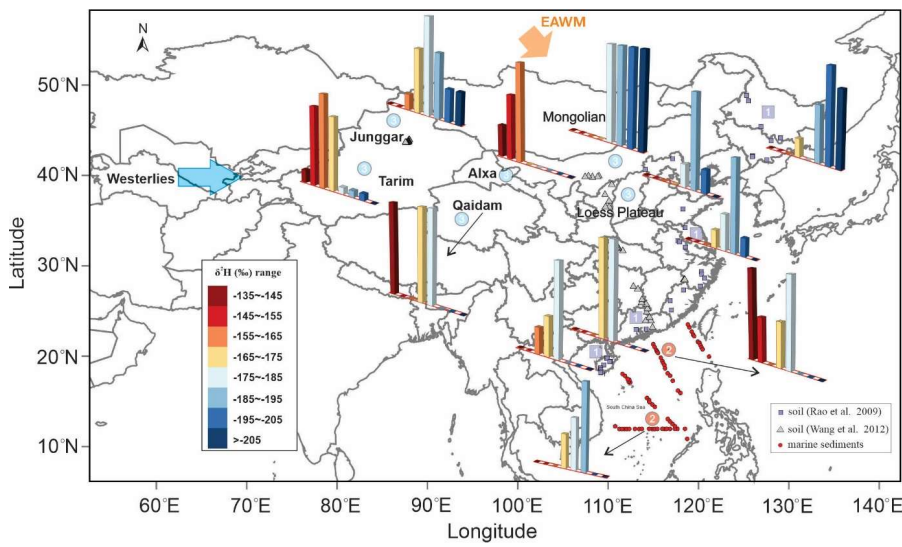
548



549 **Figure Captions**

550

551 Fig. 1 Distribution of samples used in this study: a) new surface sediment analyses from the South China
552 Sea (red dots); b) surface soil samples previously reported by Rao et al. (2009) and Luo et al. (2012) in
553 the Chinese mainland. The frequency histograms show the geographical distribution of the hydrogen
554 isotopic composition of the C₃₁ n-alkane in : 1) northeastern China (purple squares, Rao et al., 2009);
555 2) the shallow and central SCS (red circles, this study) and; 3) the Loess Plateau and Gobi deserts (blue
556 circles, this study). The sequential color gradient (from red to blue) represents heavy to light hydrogen
557 isotope values.
558



559

560

561

562

563

564

565

566

567

568

569

570

571

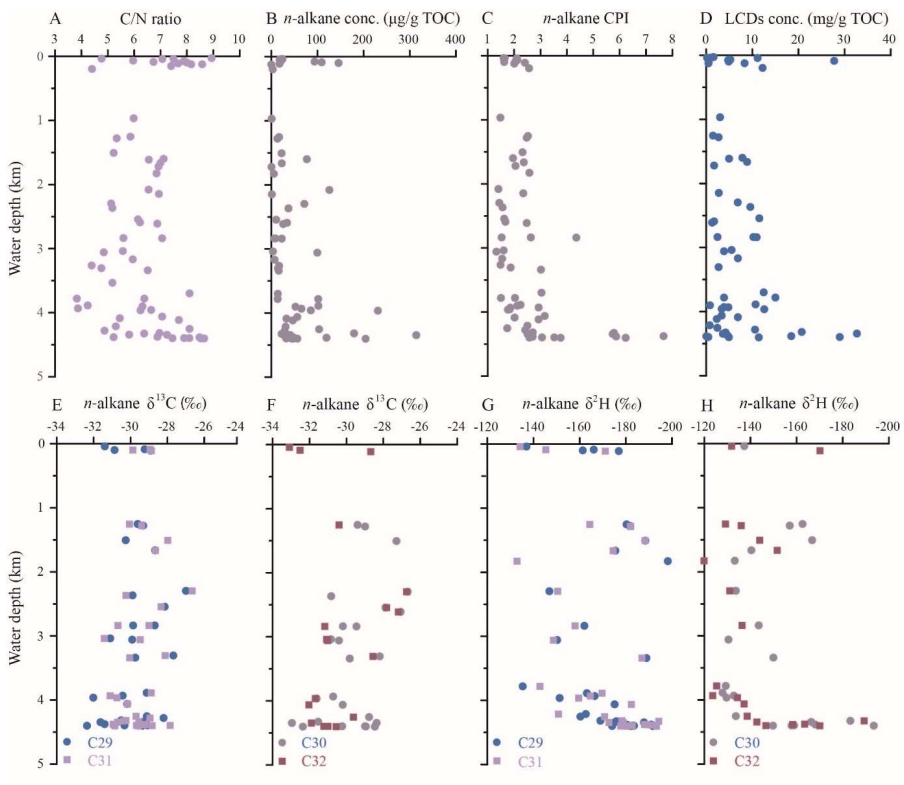
572

573

574

575

576 Fig. 2. Water depth distribution of molecular and elemental parameters measured in SCS surface
 577 sediments. Marked changes are notable at water depths below 4000 m. a) C/N ratio, b-c) Concentrations
 578 of *n*-alkanes and CPI values, d) Concentrations of long chain diols, e-h) Odd (C₂₉ and C₃₁) and even
 579 (C₃₀ and C₃₂) chains hydrogen and carbon alkane isotopes.
 580
 581



582
 583
 584
 585
 586
 587
 588
 589
 590
 591
 592
 593
 594

595

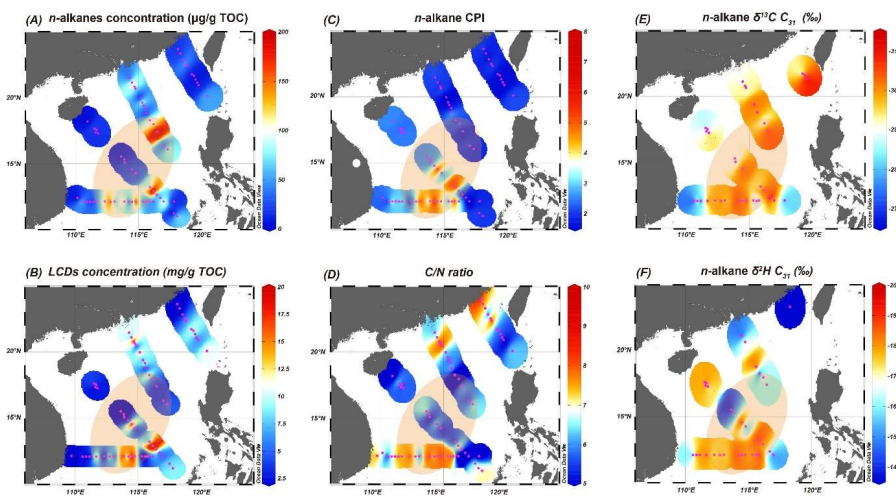
596 Fig. 3 Spatial distribution of molecular and elemental parameters from the northern to the central basin of
597 the SCS. Distinct values (e.g. high *n*-alkane concentrations, high CPI, isotopically light) are highlighted in
598 the central basin. a-b) Concentrations of *n*-alkane and long chain diols, c) *n*-alkane CPI value, d) C/N ratio,
599 e-f) carbon and hydrogen isotopes of C₃₁ *n*-alkane. The shaded circle roughly show the deep basin with water
600 depth deeper than 2400m.

601

602

603

604



605

606

607

608

609

610

611

612

613

614

615

616

617

618

619

620

621

622

623

Formatted: Font: Italic

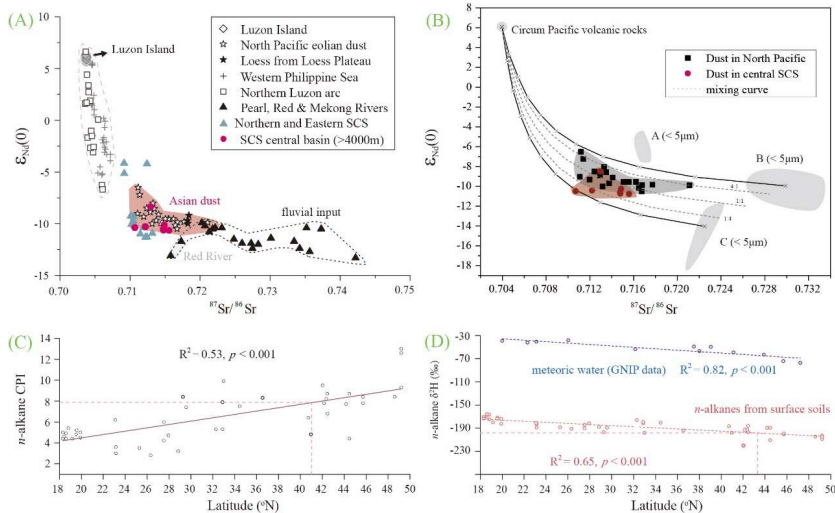
624

625 Fig. 4 Latitudinal gradients for Sr-Nd isotopes, CPI values and hydrogen isotopes of *n*-alkanes. These
626 parameters are used to infer the source of dust which has been long-range transported to the deep, central
627 basin of the SCS. A) Correlation between ϵ_{Nd} and $^{87}Sr/^{86}Sr$ of SCS surface sediments, modified from
628 Liu et al. (2014). Shaded areas show potential sources for material in the central basin. Data of the Pearl,
629 Red and Mekong rivers from Liu et al. (2007); northern Pacific ocean dust samples are from Pettke et
630 al. (2000). Luzon Arc and Luzon Island samples are from Defant et al. (1990), Philippine Sea samples
631 are from Jiang et al. (2013), Loess samples are from Chen et al. (2007). B) Sr-Nd isotopic compositions
632 of ancient dust falls in North Pacific, and SCS central basin, together with the mixing curve between
633 the $<5 \mu m$ silicate fractions of the Chinese deserts (Chen et al., 2007) and the volcanic end-member
634 used in Biscaye et al. (1997). The grey dashed lines means the mixing fraction based on end member B
635 and C C), the variation of the CPI values of the *n*-alkanes of the surface soils from different latitude
636 East China reported by Rao et al. (2009). The dashed line in red shows the maximum of CPI values
637 identified in marine sediments of the deepest water in SCS, with the interception with the regression
638 line (red line) showing the potential dust source; D), the variation of the deuterium content in meteoric
639 water (the original data are available at the website of Global Network of Isotopes in Precipitation
640 (GNIP), <http://isohis.iaea.org>) and in *n*-alkanes of surface soils in East China reported by Rao et al.
641 (2009). The lowermost perpendicular red dashed lines indicate the most depleted δ^2H values of the *n*-
642 alkanes identified in marine sediments of the deepest waters in the SCS. The interception with the
643 regression line (dashed line in blue) shows the general latitude of the potential dust source.

644

645

Commented [MOU4]: This appears also red?



646